Chapter 58

LEACHED SALT CAVERN DESIGN USING A FRACTURE CRITERION FOR ROCK SALT

Dale. S. Preece and Wolfgang R. Hawersik

Sandia National Laboratories
Albuquerque, New Mexico 87185

INTRODUCTION

In 1975 Congress passed the Energy Conservation Act to establish a U. S. Strategic Petroleum Reserve (SPR) with a capacity of 750 million barrels of crude oil. The most economic storage medium was determined to be salt caverns leached in salt domes in Louisiana and Texas. Salt caverns existed at several sites when the reserve was created. These were obtained by the U. S. Department of Energy (DOE) and used to initiate SPR oil storage. In order to meet the storage capacity approved by Congress, new caverns also had to be leached. To support the resulting design effort, finite element computer programs have been used to determine the creep closure and structural stability of salt caverns. Using site specific material properties including creep models, elastic moduli and fracture date, the finite element analyses have replaced earlier empirical approaches to cavern design. This report presents results of such finite element analyses to determine the best cavern roof shape and the minimum pillar to diameter ratio, P/D. These numerical predictions indicete that the current cavern design is safe.

FINITE ELEMENT AND MATERIAL MODELING

The finite element program used in this study has existed for approximately four years. Its theoritical basis (Key, et al, 1980) and application are well documented. It was originelly developed to predict the creep around mined openings in bedded rock salt for the Waste Isolation Pilot Plant (WIPP). The program was tested by modeling the creep of salt around a drift and by comparing the results with the predictions of eight other structural computer codes (Morgan, et al. 1981). Since then the program has had continual use for calculations to support the WIPP (Miller, et al, 1983). For about two years the

program has also been used to calculate the creep and structural stability of SPR salt caverns (Preece and Stone, 1982). Other applications include the analysis of laboratory creep tests that are used to develop creep models for salt (Branstetter and Preece, 1983).

The program numerically simulates the creep of rock salt and the resulting stresses, strains and displacements as functions of time. The constitutive model used has elastic and creep components where strain rate is a power function of effective stress as given below.

$$\dot{\bar{e}} = A\,\bar{\sigma}^{\bar{n}} \tag{1}$$

where

$$\dot{\bar{e}} = \sqrt{(2/3\ \dot{e}_{ij}\ \dot{e}_{ij})}$$

e_{ij} = plastic strain rate tensor

$$\bar{\sigma} = \sqrt{(3/2\ S_{ij}\ S_{ij})}$$

S_{ij} = deviatoric cauchy stress tensor

A = laboratory determined constant

n = laboratory determined stress exponent

The elastic constants and the creep parameters used are listed in Table I. They are based on extensive creep data on rock salt from the Salado formation in New Mexico and on limited but site specific measurements on salt samples from West Hackberry and Bryan Mound (Wawersik, et al, 1980a and 1980b). The parameters in Table I either match or overpredict the creep rates that are recorded in laboratory tests. Within the context of this study, overpredictions are considered conservative and acceptable.

TABLE I

Material Properties of Regions in Figure 3

Elastic Materiel	Youngs Modulus (Pa)*	Poisson's Ratio
Shale	7.09 E 8	.288
Caprock	7.09 E 8	.288
Overburden	9.58 E 5	.330

Salt A [$(Pa)^{4.9}$days)]$^{-1}$	N	Shear Modulus (Pa)	Bulk Modulus (Pa)
4.82 E-39	4.9	1.75 E 10	1.55 E 10

* Intact modulus (Winterkorn, 1975) divided by ten

Rock salt fracture was treated in two ways. As usual, tensile failure was described by means of a cut-off stress. In this case, the cut-off stress was set equal to zero Compressive fracture was modeled by means of a limiting inelastic strain criterion. The limiting strain, in turn, is a measure of damage before the rock ruptures in the sense that it looses some or all of its load bearing ability. At this time, the criterion does not consider the effect of fracture healing. The compressive fracture criterion used is based on empirical observations in traixial compression tests [Wawersik, 1974]. Accordingly, the axial strain to rupture, e_1^r, is given by the sum of instantaneous strains and time-dependent strains, $e_1^r = e_1^i + e_1^c$. Referring to Fig. 1, e_1^i is the inelastic strain upon loading to any stress $\tau = \sigma_1 - a3$ in the pre-failure regime. e_1^c is the time-dependent strain past e_1^i as observed, for example, in a creep test. Measurements indicate that e_1^c of salt is between the ultimate strain, e_1^u, in quasi-static tests and the quasi-static post-failure strain at the same strain rate and at the same value of σ_3 Laboratory tests on salt further suggest that the post-failure behavior of rock salt may be approximated by a line of slope β (Figure 1) that increases rapidly with the smallest principal compressive stress, σ_3, and temperature, T. Combining these observations, it was possible to write

$$e_1^r = e_1^i + e_1^c \leq e_1^u + \frac{\tau - \tau_u}{\beta} \qquad (2)$$

with, for example, $\frac{1}{\beta} = -\exp \frac{U}{T} (a\sigma_3^m + b)$. The parameters, U, a, m and b are constant. τ_u is the ultimate stress (Figure 1).

To bound rock salt failure in general, equation (2) was rewritten by expressing the least compressive stress in terms of the mean stress, σ and the effective stress, $\bar{\sigma}$, and by replacing the e_1 by $\bar{e}$, the effective strain, and τ by $\bar{\sigma}$. Thus, setting $\frac{1}{\beta} = \alpha$,

$$\bar{e}^r = \bar{e}^i + \bar{e}^c \leq \bar{e}^u + \alpha(\bar{\sigma} - \bar{\sigma}_u) \qquad (3)$$

where $a = \alpha(\sigma, \bar{\sigma}, T)$. Equation (3) may be recast in terms of strain rate by substitution of τ using the rate Eqn (1).

To evaluate the stability of caverns, it was important to be conservative. This was attempted by assuming a = 0 and using only ultimate strains that were measured at ambient temperature. Under these conditions, early laboratory compression data at strain rates $\dot{e} \approx 10^{-5}\ s^{-1}$ were fitted by a second order polynomial to yield limiting strain

$$\bar{e}^r \approx \bar{e}^u = 2.30 + (4.57 - 0.357\ \sigma_3)\sigma_3 \text{ for } \sigma_3 \leq 3.45 \text{ MPa}$$

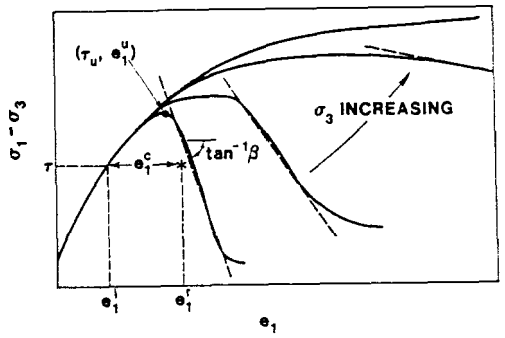

Figure 1. Schematic of Complete Quasi-Static Stress-Strain Curves, $f_{\sigma_3} - \tau_{3j}$ vs e_{1j}, and Empirical Creep Rupture Parameters for Rock Salt.

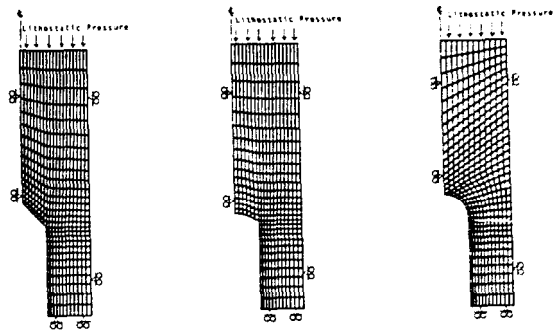

d. 45° Conical e. Parabolic f. Circular

Figure 2. Finite Element Models of Roof Configurations

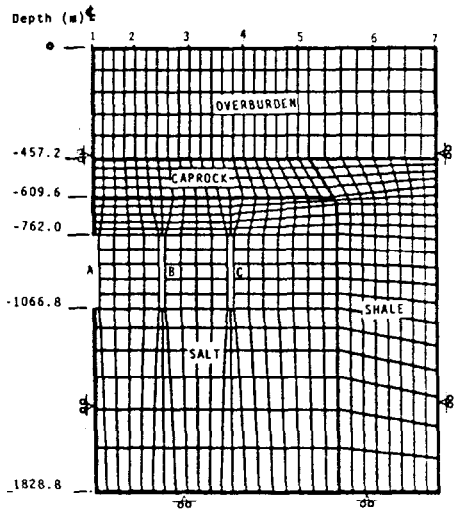

Figure 3a. Axisymmetric Finite Element Model of West Hackberry Dome with New Caverns at P/D of 1.8.

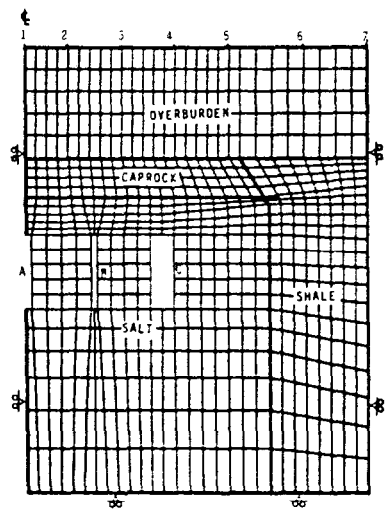

Figure 3b. Axisymmetric Finite Element Model of West Hackberry Dome with New Caverns at P/D of 1.0.

$$\bar{e}^u = 13.8 \text{ for } \sigma_3 > 3.45 \text{ MPa} \quad (4)$$

where the strain $\bar{e}^u$ is given in percent and

$$\sigma_3 = \sigma - \frac{\bar{\sigma}}{3}$$

Equation (4) was applied in the finite element analyses by comparing the calculated effective strains, $\bar{e}$, with the predicted limiting strain, $\bar{e}^u$. This comparison was done formally by means of the failure function

$$F = \bar{e} - \bar{e}^u \quad (5)$$

Stability is indicated if $F < 0$

It is important that the limiting strain and, therefore, the failure function F are deemed to be conservative, lower bound approximations. This tenet was checked by a comparison of the predicted failure strains, Eqn (4), with the failure strains of triaxial creep rupture experiments, quasi-static extension tests and more recent quasi-static triaxial measurements to 10.3 MPa confining pressure [for example, Wawersik and Hannum, 1979; Hansen and Mellegard, 1979; Price et al., 1981].

ROOF SHAPE STUDIES

The design of the roof for a new cavern resulted in choosing from the following shapes to cap a cylindrical void: 1) flat, 2) conical with angles varying 15 to 45 degrees from horizontal, 3) parabolic, and 4) spherical. The most stable roof configuration was determined by means of two different criteria: 1) the rock salt fracture criterion presented earlier, and 2) tensile stress development in the roof.

Each roof shape was analysed for 30 years of creep closure. The axisymmetric finite element mesh for each configuration is shown in Figure 2. The boundary conditions on the models are represented by rollers where motion is allowed parallel but not perpendicular to each roller. Each model has lithostatic pressure across the top. The flat roof was analysed with three different pressures inside the cavern 1) brine head pressure, 2) oil head pressure, and 3) atmospheric pressure. The brine head and oil head pressures represent maximum and minimum pressures that could occur during normal cavern operations. The atmospheric pressure case represents the most severe loading condition the cavern could ever be subjected to. The models with

conical roof angles were analysed with brine head and atmospheric pressure inside the cavern. The parabolic model was analysed with brine head pressure.

Numerical values for the two stability criterion are listed in Table II for each configuration. When compressive failure alone is considered, the flat roof appears to be the most stable roof shape since it yields the lowest value of the fracture function. This is due to a bridging effect that shifts some of the load away from the cavern roof to produce a lower creep rate. However, when the flat roof is subjected to atmospheric pressure, the minimum stress becomes tensile which makes the flat roof least desirable. The 15 and 30 degree conical configurations had compressive stresses in the roof even at atmospheric pressure. The 45 degree conical configuration at atmospheric pressure would not converge past the first several time steps. At that point, however, the stresses in the roof were well into the compressive range. In examining the fracture function values in Table II, it is noted that all are less than zero. Hence, according to this criterion, no slabbing will occur and stability at this depth is ensured.

TABLE II SUMMARY OF ROOF SHAPE STUDIES

Configuration	Type of Internal Pressure	Creep Strain At 30 Yrs (%)	Mean Stress in Roof (MPa)	Fracture Function	Minimum Principle Stress in Roof (+ Compression (MPa)
Flat	Brine Head	0.23	10.7	-13.57	8.92
"	Oil Head	0.50	9.98	-13.3	6.79
"	Atmosphere	6.7	5.26	- 7.1	-0.126
15° Conical	Brine Head	0.31	11.7	-13.49	8.92
"	Atmospheric	9.80	6.09	- 4.0	0.0163
Parabolic	Brine Head	0.35	11.7	-13.45	8.988
30° Conical	"	0.43	16.7	-13.37	9.01
"	Atmospheric	14.0	6.88	- 0.20	0.427
45° Conical	Brine Head	0.65	11.7	-13.15	9.07
"	Atmospheric	- - -	- - -	- - -	8.20
Circular	Brine Head	6.75	11.8	- 7.05	9.41

PILLAR TO DIAMETER RATIO

The ratio of pillar to cavern diameters (P/D) was evaluated by means of two criteria. (1) the absence of fracture in tension or compression, and (2) the percent volume loss of the cavern due to creep closure. These criteria were applied in the analysis of a new cavern array that was adopted for several SPR facilities currently under construction.

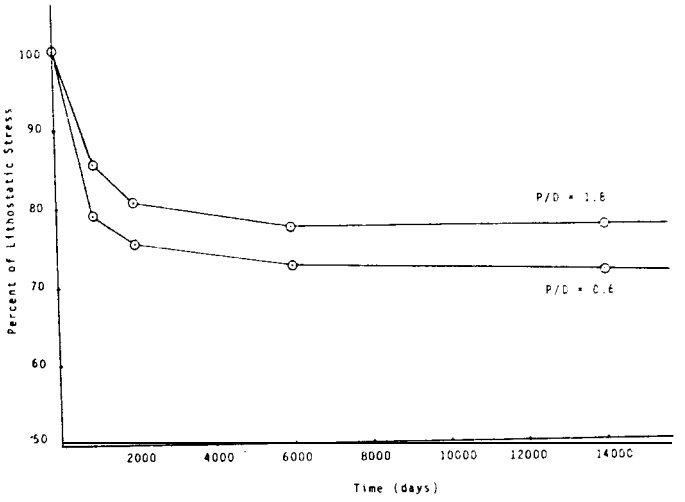

Figure 4. Vertical Stress History 152 Meters Above Toroid B.

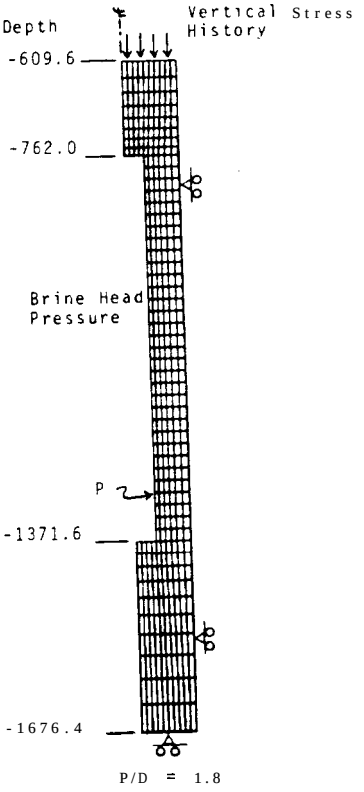

Figure 5. Detailed Axisymnetric Finite Element Model of a Cylindrical Cavern.

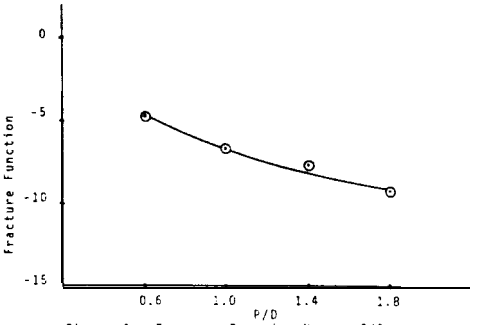

Figure 6. Fracture Function Versus P/D.

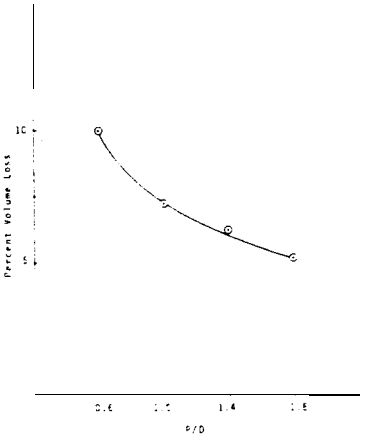

Figure 7. Percent Volume Loss versus P/D

Two analyses were carried out. The first was a simplified but large scale axisymmtric model of the entire dome to investigate coupling between the structural response of individual caverns and the entire salt dome. It showed that, due to creep relief, the stresses around the caverns are reduced from the original lithostatic stress as some of the overburden load is shifted to the caprock or transfered to the shale and sand layers along the sides of the dome. The computed stresses from the large-scale model were then used to set the boundry conditions for a more detailed analysis of the actual cavern complex. The large scale finite element model is shown in Figure 3a. Both sides of the model were allowed to move vertically but not horizontally. The bottom is allowed to move horizontally but not vertically. The top, which represents the ground surface, is unconstrained. The four different materials included in the model are labeled on the mesh and their corresponding properties are given in Table I. The low moduli for shale, caprock and overburden accounted for discontinuities in the rock, consistent with some subsidence predactions using linear elastic finite elements (Dahl and Choi, 1973). The caverns were modeled as a central cylinder, "A" surrounded by two toroids "B" and "C". The cylinder and toroids are configured to approximate the volume and volumetric distribution of the actual West Hackberry SPR site.

The model also approximated the entire history of the cavern complex from the creation of the first caverns in 1940 to the caverns currently being leached. Starting with lithostatic stresses everywhere, the pressure in cylinder "A" and toroid "B" was lowered gradually to brine head pressure over 4000 days (11 years) to simulate the first leaching phase. The computation was continued at constant brinehead pressure within caverns "A" and "B" until, after 11,000 days (30 years) leaching of the new caverns was simulated by reducing the pressure in torroid "C" to simulate leaching the new caverns. Gradual depressurization of "C" occurs over 3000 days (8 years) and is followed by constant pressure conditions for 30 years, the projected life of the SPR.

Because of creep relief, the vertical stress in the region immediately above the caverns decreases as some of the overburden load shifts to the shale surrounding the dome. The vertical stress in the shale increases as a result of this load transfer. Cavern analysis which uses the original lithostatic stress above the cavern as a boundry condition will overpredict the closure of the cavern. The vertical stress history 152 meters above toroid "B" represents an average for the region above the caverns. This history, shown in Figure 4, was applied across the top of the detailed axisymmetric finite element models of the new caverns shown in Figure 5. To evaluate the pillar to diameter ratio, P/D was varied from 1.8 to 0.6 by changing the mesh width while the cavern radius remained constant. Each model had the vertical stress history from the previous analysis across the top and brine head pressure inside the cavern. These models were analysed for 30 years and the results were post-processed for stability and volume change.

The cavern stability was evaluated by means of the fracture function. "F" Eqn (5). Values of "F" were calculated by post-processing the creep strains and stresses from each analysis. Accordingly, "F" varies vertically along the cavern wall and is at a maximum at approximately point "P" shown in Figure 5. Values of the fracture function at "P" in each model after 30 years of creep is shown in Figure 6 as a function of P/D. The plot indicates that all pillar widths are predicted to be stable.

The cavern volume decreases with time due to creep closure. The calculated volume loss for each cavern after 30 years of closure is shown in Figure 7 as a function of P/D. Figure 7 indicates that the volume loss from the caverns is within acceptable limits when the P/D is reduced.

CONCLUSIONS

The results of several finite element analyses of salt creep and fracture around SPR caverns are consistent with the pillar to diameter ratio of 1.8 that is currently applied to the design of SPR caverns. The calculations further indicate that this spacing has an adequate but not overly conservative safety factor of approximately two. Moderate reductions of P/D from 1.8 should not result in cavern collapse. To ensure cavern stability along the roof, conical shapes with roof angles between 15 and 30 degrees appear to be optimal. In the future, it is planned to also evaluate the effect of P/D = 1.8 on the magnitude of surface subsidence at each SPR site.

REFERENCES

Branstetter, L. J. and Preece, D. S., 1983, " Numerical Studies of Laboratory Triaxial Creep Tests," Proceedings of 24th Symposium on Rock Mechanics, Texas A & M University.

Dahl, H. D. and Choi, D. S., 1973, " Some Case Studies of Mine Subsidence and its Mathematical Modeling," Proceedings of 15th Symposium on Rock Mechanics, South Dakota,

Hansen, F. D. and Mellegard, K. D., 1979, " Creep Behavior of Bedded Salt from Southeastern New Mexico," RE/SPEC Inc. RSI-0062, 1977; Sandia National Laboratories, SAND79-7030.

Key, S. W., Stone, C. M. and Krieg, R. D., 1980, " A Solution Strategy for the Quasi-Static Large Deformation, Inelastic Response of Axisymmetric Solids," presented at U. S. European Workshop Nonlinear Finite Element Analysis in Structural Mechanics, Ruhr-Universitat; Bochum, West Germany.

Morgan, H. S., Krieg, R. D. and Matalucci, R. V., 1981, " Comparitive Analysis of Nine Structural Codes Used in the Second WIPP Benchmark Problem, " Sandia National Laboratories, SAND81-1389.

Miller, J. D., Stone, C. M., and Branstetter, L. J., 1982, " Reference Calculations For Underground Rooms of the WIPP ", Sandia National Laboratories, SAND82 - 1176.

Preece, D. S. and Stone, C. M., 1982, " Verification of Finite Element Methods Used to Predict Creep Closure of Leached Salt Caverns," Proceedings of 23rd Symposium on Rock Mechanics, Berkeley Calif.

Price, R. H., Wawersik, W. R., Hannum, D. W., and Zirzow, J. A., "Quasi-Static Rock Mechanics Data for Rocksalt from Three Strategic Petroleum Reserve Domes," Sandia National Laboratories, SAND81-2521, 1981.

Wawersik, W. R., Hannum, D. W. and Lauson, H. S., 1980a, " Compression and Extension Data for Dome Salt from West Hackberry, Lousiana, Sandia National Laboratories, SAND79-0668.

Wawersik, W. R., Holcomb, D. J., Hannum, D. W. and Lauson, H. S., 1880b, "Quasi-Static and Creep Data for Dome Salt From Bryan Mound, Texas, Sandia National Laboratories, SAND80-1434.

Wawersik, W. R., "Creep Fracture of Rock," Proceedings of Fourth International Symposium on Rock Mechanics, Denver, Colorado, 1974

Wawersik, W. R., "Interim Summary of Sandia Creep Experiments on Rock Salt from the WIPP Study Area, Southeastern New Mexico," Sandia National Laboratories, SAND79-0115, 1979.